Low energy (e,2e) studies of the noble gases in the perpendicular plane

Kate L Nixon, Andrew James Murray, Christian Kaiser

Low energy (e,2e) studies of the noble gases in the perpendicular plane.

Kate L Nixon[*], Andrew James Murray[§] and Christian Kaiser.

Photon Science Institute, School of Physics and Astronomy, University of Manchester, Manchester M13 9PL, United Kingdom.

Email: [*]Kate.Nixon-2@manchester.ac.uk ; [§]Andrew.Murray@manchester.ac.uk

Abstract: Detailed (e,2e) studies of the electron impact ionization of the noble gases helium, neon, argon, krypton and xenon have been carried out from near threshold to intermediate energies, where the outgoing electrons carry equal energy from the interaction. The experiments were conducted in the perpendicular plane, where the outgoing electrons are both detected orthogonal to the incident electron beam. For electrons to emerge in this geometry they must undergo multiple scattering, including scattering from the nucleus of the target, and so this geometry provides a highly sensitive test of the most sophisticated scattering theories. The data show the cross sections undergo complex variations as a function of incident energy, and in particular ionization of the heaviest target is at variance to all others that have been studied here.

PACS No. 34.80.Dp

1.0 Introduction.

The (e,2e) process provides the most precise experimental data for the study of the ionization of atomic and molecular targets by electron impact [1]. In these experiments a single electron of well defined momentum impacts with a target in the interaction region, resulting in target ionization and a scattered and an ejected electron which emerge after the interaction has taken place. By determining the momenta of the scattered and ejected electrons in a time correlated coincidence measurement, the differential ionization cross section (DCS) is derived for comparison with theoretical models.

Since the scattered and ejected electrons may emerge over a wide range of different angles, experiments usually define a specific scattering geometry in which to carry out the measurements. In Manchester, the (e,2e) apparatus can access a wide range of geometries from a coplanar geometry, where the incident, scattered and ejected electrons all occupy the same plane, through to the perpendicular geometry, where the scattered and ejected electrons emerge in a plane orthogonal to the incident electron trajectory, as shown in figure 1. Hence it is possible to accumulate a full range of DCS measurements over all scattering angles using this spectrometer [2,3].

In the present work, we have constrained the spectrometer to measure the DCS only in the perpendicular geometry, where $\psi = 90°$ as in figure 1. For both electrons to emerge in this geometry it is necessary for

multiple scattering to occur, where the incident electron strongly interacts with both the target nucleus and with the bound electrons. We have further constrained the outgoing electron energies to be equal, so that the effects of exchange between the electrons also plays an important role in the interaction. The perpendicular plane hence provides a stringent test of current ionization models. Further, we have taken measurements with the incident electron energy (E_0) ranging from near the ionization threshold of the selected target, through to energies up to 80eV above the ionization potential (IP). In this regime the probability of single ionization is a maximum, and so it is here that most ionizing collisions with electrons occur in nature. Understanding these processes is hence important in areas ranging from the production of plasmas in stellar and planetary atmospheres, through to electron impact ionization in lasers and in nuclear reactors. Low energy electron ionization has also been attributed to the production of DNA damage in biological tissue [4], and so it is important to understand these collisions at a fundamental level to describe the physics of these processes.

Unfortunately in this energy regime the demands on sophisticated quantum models of the ionizing collision are also greatest. In these models it is necessary to consider multiple collisions, target polarization, distortions of the wave-functions defining the target and the electrons, and post-collisional interactions in order to produce theoretical cross sections which agree with experimental measurements. There has been excellent success in recent years in theoretically understanding ionization of the simplest targets (eg atomic H and He) using distorted wave Born approximations (DWBA), convergent close coupling (CCC) techniques, time dependent close coupling (TDCC) techniques and other methods [5-10]. Agreement between theory and experiment has however been less satisfactory for the more complex targets, including that of molecules, although again progress has been forthcoming over the last few years for the simpler diatomic systems [11-15].

To progress these studies beyond simple atomic targets, we decided to make a systematic study of ionization for the non-radioactive noble gas targets, as is detailed in this paper. We hence present results for ionization of helium from 3eV to 80eV above the IP (24.6eV), results for ionization of neon from 5eV to 50eV above the IP (21.6eV), results for ionization of argon from 2eV to 50eV above the IP (15.8eV), results for ionization of krypton from 2eV to 50eV above the IP (14.0eV), and finally results for ionization of xenon from 2eV to 70eV above the IP (~12.1eV). For xenon, we were able to resolve the $^2P_{1/2}$ and $^2P_{3/2}$ ion states for incident energies up to 30eV above the IP, and so we also present examples of the measured DCS from these individual studies. In all cases results are presented for the outgoing electrons having equal energies at the analysers. The helium results are reproduced from previous studies carried out in Manchester [2, 16-19], and are given here for completeness.

This paper is presented in four sections. Following this introduction the apparatus at Manchester is briefly described, and the experimental conditions chosen for these studies are detailed. Results for ionization of the different noble gas targets are then presented, followed by a discussion of these data. Finally, a summary of the differences seen from individual targets is given, so as to promote discussion in the future.

2.0 The experimental configuration.

The experimental apparatus in Manchester has been detailed in a series of papers since being commissioned in 1990 (see [20] for example). As noted above, the apparatus can measure the DCS from the coplanar to the perpendicular plane geometry by moving the electron gun, gas jet and Faraday cup together around the interaction region (figure 2). This is accomplished by mounting these components on a yoke which has its rotation axis through the interaction region. A photomultiplier tube is also fixed to this assembly so that photons emitted at 450nm ± 50nm from the electron-target interaction can be counted (all targets studied here produce photons in this regime when excited by electron impact). By observing the flux of emitted photons, the electron beam can then be correctly focussed and steered onto the physical centre of rotation of both analysers and electron gun.

The electron analysers consist of a 3-element electrostatic lens that focuses electrons from the interaction region into a hemispherical energy selector. By choosing the analyser residual energy to pass electrons around the selector, a channel electron multiplier detects electrons of the specified energy for subsequent amplification and counting. In the experiments carried out here, both detectors are set to measure electrons of equal energy, given by $E_1 = E_2 = (E_0 - IP)/2$. The combined coincidence energy resolution of the unselected energy electron gun and the analysers is ~1eV, as measured from coincidence energy spectra obtained during these measurements. This resolution arises from the energy spread of the unselected electron gun and the resolution of the energy analysers.

The angular range of the measured DCS is dictated by the physical size of the analysers. In the perpendicular plane, only the mutual angle $\phi = \xi_1 + \xi_2$ is relevant, where ξ_1 and ξ_2 are as shown in figure 1. For the helium data presented here, the angular range was from $\phi = 50° - 310°$, whereas for all other targets this range was from $\phi = 70° - 290°$. This difference arises due to the redesign and installation of new analyser shields in between the time the helium measurements were taken and those measurements for all other targets presented here. The angular resolution of the spectrometer is estimated to be $\Delta\phi = \pm 5°$ in this plane, as calculated from the entrance apertures of the individual analyser electrostatic lenses.

The data were taken over a period of several months, and the electron gun current was varied for each of the data sets so as to ensure linearity of the detection system and a reasonable coincidence count rate compared to the random background signal. At these low electron energies it is very difficult to accurately determine the size and shape of the incident electron beam, and therefore its overlap with the target, which would allow a relative normalisation over the different selected energies. The data are hence normalised to unity at the peak of the DCS at each energy. The shape of the DCS for a given energy and target is then of importance, for comparison with future theoretical work.

The energies of the incident and scattered electrons in the spectrometer were independently determined by measuring resonances in elastic and inelastic scattering data. The energy of the incident electron beam was determined by observing the negative ion elastic scattering resonance in helium at ~19eV, so as to determine the offset in the gun due to contact potentials. The energies of the outgoing electrons were determined by observing inelastic scattering from the excited targets, and by considering the location of Fano resonances in the ionization continuum.

3.0 The experimental data.

The experimental data for helium are taken from previous work carried out in Manchester [2, 16-19]. These are re-presented here normalised to unity at the peak of the DCS to allow a comparison between this target and the other noble gases. The ground state of helium is $^1S_0$, with an electronic configuration $1s^2$, and so both bound electrons occupy s-shell orbitals prior to the interaction. The orbital angular momentum of each electron is hence zero, with a momentum distribution that peaks around zero a.u.. This contrasts with the other noble gas targets whose ground states are also $^1S_0$, but whose valence electrons occupy closed p-orbitals. In these cases the momentum probability of the p-electron is a maximum at a non-zero value [1], with this value depending upon the particular target under study.

For helium, neon and argon targets, the bound electrons occupy either s-orbitals or p-orbitals in their ground state. The configuration of the 10 electrons in neon is $1s^2 2s^2 2p^6$, whereas argon has 18 electrons occupying a configuration $[Ne]3s^2 3p^6$. By contrast, the bound electrons in both of the heavier targets also occupy d-orbitals, with a correspondingly more complex momentum distribution. Krypton has 36 electrons and has a ground state configuration $[Ar]3d^{10}4s^2 4p^6$, while xenon has 54 electrons with a ground state configuration $[Kr]4d^{10}5s^2 5p^6$.

For all noble gas targets except helium, the removal of the valence p-electron during ionization leaves the ion in two possible ground states, either the $^2P_{1/2}$ ion state or the $^2P_{3/2}$ ion state. It was not possible to resolve these individual channels in our experiment (due to the limited energy resolution of the spectrometer) apart from that for xenon, where results were taken for production of the two different ion

states at incident electron energies from 10eV to 30eV above the IP. Results from the measurements to these individual ions states are given in section 3.5 below.

3.1 Helium.

Figure 3 presents the results for ionization of helium in the perpendicular plane for ten different incident energies ranging from 3eV to 80eV above the IP. At the lowest energy only a single broad peak occurs centred around $\phi = 180°$. This is considered to be due to the dominance of post-collisional interactions (PCI) between the outgoing electrons, which drives electrons emerging with equal energies from the interaction region asymptotically towards opposite directions. As the outgoing electron energy is lowered, the post-collisional interaction time increases, resulting in an increased flux in the $\phi = 180°$ direction. This type of threshold behaviour was first predicted by Wannier [21] and was later considered by Peterkop, Rau and others [22-24] to explain results in this regime.

As the incident electron energy increases, additional peaks are seen at angles $\phi \approx$ 90° and 270°. These peaks are mirror images of each other due to symmetries in the perpendicular plane. By 20eV above the IP three distinct peaks are clearly visible, the relative strength of the central peak to outer lobes decreasing monotonically as the energy increases. At ~50eV excess energy the three lobes have equal amplitudes, whereas at higher energies the outer lobes dominate. At excess energies over 80eV above the IP the central lobe has virtually disappeared, leaving only the two outer lobes in the DCS.

The physical reasons behind these structures has been described by several different models, ranging from DWBA calculations through to TDCC models [5,8,10]. The DWBA theory most easily allows the different processes involved in the interaction to be 'switched' on and off, and this has explained the origin of these lobes. There is only one process that can produce a peak at $\phi = 180°$ in the perpendicular plane without interaction with the target nucleus. This process requires the momentum of the incident electron to be exactly matched by the momentum of the bound electron, with both electrons moving in opposite directions prior to the interaction. In this case, momentum conservation requires the outgoing electrons to move in opposite directions ($\phi = 180°$) in the perpendicular plane. This mechanism was considered as being the main reason for the peak at $\phi = 180°$ until the work of Madison and co-workers in 2009 [25] showed the probability of this occurring was low. They then proposed a *triple* scattering mechanism to describe this peak, where the incident electron first scatters elastically from the nucleus so as to enter the detection plane, followed by a binary inelastic collision with a bound electron, followed by elastic scattering of one of the electrons back from the nucleus. This complex mechanism was found to emulate the cross section more closely compared to the single scattering process originally envisaged [17].

The peaks at $\phi \approx 90°$ and 270° were further found to result from elastic scattering of the incident electron from the core, followed by a single binary collision between the incident electron and a bound electron. In this case, since the particles have equal mass and energy, they emerge from the interaction region at a mutual angle $\phi \approx 90°$ (or $\phi \approx 270°$), as is observed. DWBA, CCC and TDCC models all now reproduce the data from these helium experiments relatively accurately in this plane. It is therefore widely considered that the principle physics behind these ionization processes is well known.

It should be noted that although agreement between theory and experiment in the perpendicular plane has proven to be very good, the results in a coplanar geometry are not as satisfactory, particularly for non-equal outgoing electron energies [26]. It is therefore clear that further work is needed to fully describe the ionization reaction, even for a simple target like helium.

3.2 Neon.

The new results for the ionization of neon are shown in figure 4. The lowest energy studied was 5eV above the IP, with six measurements being taken up to 50eV above the IP as shown. The results at the lowest energy are similar in shape to that for helium, with a single broad peak observed centred around $\phi = 180°$. The width for this peak in neon is ~120°, which is broader than the ~80° for the same outgoing electron energy in helium. The DCS shows no additional lobes at this energy.

As the incident energy increases, the DCS for neon shows a very different character to that for helium. As the energy is raised to 10eV above the IP, the broad single peak seen at the lowest energy increases in width, and develops a flat structure at the peak. At 15eV above the IP this flat structure has evolved into two peaks with $\phi = 180°$ now being a local *minimum*. As the energy increases further, the peaks separate in angle, and the minimum at $\phi = 180°$ deepens. At the highest energy studied (50eV above the IP), the magnitude of this minimum is smaller than at the highest and lowest angles measured ($\phi = 70°, 290°$). As for all measurements in this study, the DCS must be zero for the electrons emerging at the same angle ($\phi = 0°, 360°$), due to post-collisional interactions between outgoing electrons of equal energy.

The mechanisms that produce these structures in neon must be quite different to that proposed for helium, apart from at the lowest energy where PCI is expected to dominate for all targets, as predicted by Wannier and others [21-23]. Al-Hagan and co-workers [24] recently considered the low energy regime for both He and H_2 from threshold to ~10eV above threshold, and concluded that for these targets PCI dominates at energies <2eV, which is also consistent with the observations for neon presented here. However, at higher energies the mechanisms proposed for helium ionization described above would be expected to produce similar structures in all targets that have a central ionic core. The results in figure 4

indicate that the interaction is clearly more complex, and may be due to the momentum distribution of the ionized p-electron and polarizability of the atom (which is 1.9 times greater for neon than for helium) [28]. It is clear that further theoretical calculations are required to establish what these mechanisms are.

3.3 Argon.

A similar study was carried out for an argon target, whose outer electronic structure ([Ne]$3s^2 3p^6$) is similar to neon ([He]$2s^2 2p^6$). The calculated atomic radius of argon (71pm) is however significantly larger than that for helium (31pm) or neon (38pm) due to the n=3 shell being occupied [27]. The static polarization of argon is eight times larger than for helium, so scattering effects due to polarization of the target are expected to be significantly larger than for neon or helium. A summary of the radii and polarization of the different targets is given in table 1 [27,28]. In the frozen-core approximation, as used in many theories, the inner electrons are considered as 'spectators' during the interaction, and so in this approximation the structure of the DCS should be similar for neon and argon. The results presented in figure 5 however show this is not the case.

For argon, nine separate energies were chosen for study, so as to reveal the complex variation in the DCS as a function of energy. The lowest energy studied was 2eV above the IP, the data at this energy having poor statistics due to experimental difficulties working with argon at this energy. However, these data show that there is an approximate 3-lobe structure to the DCS, with the result at $\phi = 180°$ being of similar magnitude to that around $\phi \approx 90°$ and 270°. It is likely that PCI is again dominating at this energy, in support of the Wannier model. The physical 'size' of this target compared to helium and neon may also act to partially shield the outgoing electrons which are emerging at $\phi = 180°$, thereby rendering the effects of PCI to be less significant compared to helium and neon. Raising the electron energy to 5eV above the IP produces much better statistics, and at this energy there is now a *minimum* at $\phi = 180°$ in contrast to helium and neon, with clear side lobes at $\phi \approx 110°$ and 250°. This minimum flattens at 10eV above the IP and rapidly evolves into a clear peak 15eV above the IP. This central peak is visible for incident energies up to 40eV above the IP, until at the highest energy (50eV above the IP) this has once again disappeared, the side peaks having also moved outwards compared to the lower energies. This angular shift of the side lobes is consistent with PCI playing a continuing role in the interaction, since as the energy increases the effects of PCI diminish and the electrons move away from $\phi = 180°$, as is observed.

Once again the results for argon are not consistent with the simple models found successful for helium. The results further indicate that the use of a 'frozen-core' approximation is unlikely to be accurate in any

theory attempting to emulate these data, and that future models will need to consider multiple interactions with all bound electrons to accurately describe the process in this target. This is likely to put severe demands on model calculations in the future.

3.4 Krypton.

Figure 6 shows the results for krypton, which unlike helium, argon and neon also has bound electrons occupying the 3d-shell. The physical 'size' of krypton (88pm) is slightly larger than argon due to occupation of this shell, and due to closed occupation of the 4s and 4p shells. The static polarization of krypton is ~1.5 times that of argon, as shown in table 1 [27,28].

Once again results were taken for a lowest energy of 2eV above the IP, with the data having much better statistical significance compared to those for argon at the same outgoing electron energy. Ionization of krypton no longer shows the dominance of PCI as predicted by Wannier, since there is now a central *minimum* at $\phi = 180°$. The relative magnitude of this minimum compared to the peaks around $\phi = 110°$ and 250° is however larger than for higher incident energies, so there is probably a contribution to the cross section at this angle due to PCI. As the energy increases, the results for krypton show a similar trend to that for argon, with the central minimum deepening until around 10eV above the IP where a central peak starts to emerge. This central peak is not as significant in krypton compared to the side lobes, and by 30eV above the IP it is once again diminishing. This central peak has virtually disappeared at 40eV above the IP and there is no evidence of a peak by 50eV above the IP.

The similarity between argon and krypton data tends to indicate that the d-shell electrons in the heavier target are not playing a significant role in the ionization process. It also appears that the variation in cross section as a function of energy follows a similar pattern for each of these targets. It might hence be expected that the cross section for the heaviest target (xenon) would follow a similar trend to that of argon and krypton.

3.5 Xenon.

As the heaviest isotopically stable noble gas target, xenon has the largest calculated 'size' (108 pm) due to full occupation of the 4d, 5s and 5p shells [27]. The static polarizability of xenon is also highest, being ~1.6 times greater than krypton [28]. The ionic ground states of Xe^+ are sufficiently separated that it was possible to resolve ionization to the individual states during the experiments, for energies up to 30eV above the IP. A coincidence energy loss spectrum is shown in figure 7 to illustrate this separation at an incident electron energy 10eV above the IP for this target. The data show that the spectrometer can

reasonably resolve the ionization to each ionic ground state, and that ionization to the $^2P_{3/2}$ ionic ground state is ~2.3 times more likely than to the $^2P_{1/2}$ ground state at this energy. It was only possible to resolve these states at energies up to 30eV above the IP. Above this energy the data measured will have contributions from both states. It is anticipated, however, that the measured data will still be dominated by the $^2P_{3/2}$ state.

Figure 8 shows the coincidence data for the DCS obtained from ionization of xenon to the $^2P_{3/2}$ ion state. The results were taken from 2eV above the IP to 70eV above the IP for this target, so as to establish the variation in the cross section that is observed. The data are particularly surprising since they do *not* follow the general trend seen for all other noble gas targets at higher energies. At the lowest energy 2eV above the IP, a clear two-peak structure is observed which is similar to that observed from krypton. This indicates that PCI is once again *not* the dominant mechanism producing the cross section at this energy.

The minimum at $\phi = 180°$ is significantly deeper than for krypton under the same outgoing energy conditions, and unlike krypton this minimum then becomes shallower as the incident energy increases. At 7eV above the IP a peak is clearly resolved at $\phi = 180°$. The relative magnitude of this peak compared to the lobes at $\phi \approx 110°$ and 250° then increases in magnitude as the energy increases, as with krypton and argon. However, unlike krypton and argon whose central peak reaches a maximum and then decreases, the central peak in xenon continues to dominate the cross section as the energy rises. This trend continues up to the highest energy which was possible to measure (70eV above the IP), where the central peak is seen to be broad with a width ~100°. At all energies greater than 40eV above the IP, the outer peaks seen in all other targets have disappeared.

These results show that the mechanism for ionization of xenon must once again be different to all other targets that have been studied. The results at higher energies are surprising, as the mechanism that produces the central peak with the electrons moving opposite each other is clearly dominating over all the other scattering processes. As far as we are aware this phenomenon has never been observed for any other target, and it remains to be seen why this should occur for xenon. Clearly theoretical input is urgently required to explain this unusual result.

Figure 9 finally shows the results obtained for ionization of xenon resulting in the $^2P_{1/2}$ Xe^+ ion state, compared to that resulting in the $^2P_{3/2}$ state for the same outgoing electron energies. Only three energies were selected for these experiments, due to the difficulty of obtaining good statistical data. These data indicate that fine structure in the final ion state does not play a significant role in the ionization process, since the comparison between this data and that reproduced from figure 8 shows that the shapes of the

cross section for each energy are very similar. This result indicates that fine structure does not appear to play a significant role in electron collision processes at these energies.

4.0 Discussion and summary.

The comprehensive set of data presented in this paper for the isotopically stable noble gases have shown there is a large variation in the probability of ionization in the perpendicular plane, which needs to be explained by future theoretical calculations. The perpendicular plane is particularly poignant for testing the most sophisticated electron impact ionization models, since multiple scattering must occur for electrons to emerge in this plane. This contrasts to the coplanar geometry most often adopted, where the dominant scattering mechanism is usually a single binary scattering between electrons, resulting in a high probability that forward scattering occurs.

The perpendicular plane has proven to be a fertile ground for several recent theoretical models, which have found success for simple targets such as helium and molecular hydrogen. The results presented here will hence further test these models for heavier targets, so as to elucidate the scattering mechanisms that result in the observations. The marked contrast between results for helium and all other noble gas targets demand that these models carefully consider the intricacies of the interaction, since a simple extension of the basic physical ideas presented for helium cannot explain the experimental data. Further, the ‘frozen core’ approximation often adopted in these models which treat all non-ionized electrons as spectators does not appear valid for the heavier targets when compared to neon, even thought the outer valence electrons have the same p-type character. It is hence likely that these assumptions will need to be relaxed to accurately model the data.

Even though the results for each target vary widely, similarities are also observed. In particular, it appears that PCI plays a role at the lowest measured energy for each target, although the significance of this process reduces as the target weight increases. Argon, krypton and xenon also all evolve a central peak as the incident electron energy increases from near threshold, which cannot be due to PCI. For argon and krypton the relative magnitude of this peak increases with respect to the side lobes until it reaches a maximum, then decreases to become insignificant at the highest energies measured.

The most surprising result is for the heaviest target xenon, since the relative magnitude of the central peak continues to increase as the incident energy increases, and the side lobes reduce to insignificance. The side lobes observed previously in the perpendicular plane have been attributed to a binary collision between the incident electron elastically scattered into this plane and a bound electron. This process has always been considered as the dominant mechanism at higher incident energies, yet the new results presented here indicate these ideas need to be revisited for this heavy target.

It is finally worth noting that the resolved data for ionization to the $^2P_{3/2}$ and $^2P_{1/2}$ Xe^+ states indicate there is little variation to the measured cross section due to fine structure effects. It is hence likely that the results for neon, argon and krypton are also not significantly altered by these effects, even though the spectrometer was not capable of resolving their individual ion states.

In summary, we have presented a comprehensive set of experimental data in the perpendicular plane for the noble gases, ranging from near threshold to energies up to 80eV above the ionization potential for these targets. The results indicate that the interaction is complex, that it depends on the selected target and that the approximations used to successfully predict the cross section for lighter targets are unlikely to remain applicable for the more complex targets. These data present a significant challenge to current scattering theories, and it is hoped that the energy range we have spanned in these experiments will allow different models to be applied to the data, so as to explain the physical complexities behind these results.

Acknowledgements.

KLN would like to thank the Royal Society for an International Newton Research Fellowship held at the University of Manchester. CK would like to thank the University of Manchester for providing a PhD scholarship while carrying out this work.

References.

[1] Weigold E and McCarthy I E 1999 *Electron Momentum Spectroscopy* (Dordrecht: Kluwer)
[2] Murray A J and Read F H 1993 *Phys. Rev.* A **47** 3724
[3] Murray A J, Bowring N J and Read F H 1997 *J. Phys.* B **30** 387
[4] Boudaiffa B, Cloutier P, Hunting D, Huels M A and Sanche L 2000 *Science* **287** 1658
[5] Zhang X, Whelan C T and Walters H R J 1990 *J. Phys.* B **23** L173
[6] Rescigno T N, Baertschy M, Isaacs W A and McCurdy C W 1999 *Science* **286** 2474
[7] Bray I, Bartschat K and Stelbovics A T 2003 *Phys. Rev.* A **67** 060704
[8] Stelbovics A T, Bray I, Fursa D V and Bartschat K 2005 *Phys. Rev.* A **71** 052716
[9] Colgan J and Pindzola M S 2006 *Phys. Rev.* A **74** 012713
[10] Colgan J, Pindzola M S, Childers G and Khakoo M 2006 *Phys. Rev.* A **73** 042710
[11] Gao J, Madison D H, Peacher J L, Murray A J and Hussey M J 2006 *J. Chem. Phys.* **124** 194306
[12] Murray A J, Hussey M J, Gao J and Madison D H 2006 *J. Phys.* B **39** 3945
[13] Colgan J, Pindzola M S, Robicheaux F, Kaiser C, Murray A J and Madison D H 2008 *Phys. Rev. Lett.* **101** 233201
[14] Colgan J, Al-Hagan O, Madison D H, Kaiser C, Murray A J and Pindzola M S 2009 *Phys. Rev.* A **79** 052704
[15] Colgan J, Al-Hagan O, Madison D H, Murray A J and Pindzola M S 2009 *J. Phys.* B **42** 171001
[16] Murray A J and Read F H 1992 *Phys. Rev. Lett.* **69** 2912
[17] Murray A J, Woolf M B J and Read F H 1992 *J. Phys.* B **25** 3021
[18] Bowring N J, Murray A J and Read F H 1997 *J. Phys.* B **30** L671
[19] Murray A J, Bowring N J and Read F H 2000 *J. Phys.* B **33** 2859
[20] Murray A J, Turton B C H & Read F H 1992 *Rev. Sci. Instrum.* **63** 3346
[21] Wannier G H 1953 *Phys. Rev.* **90** 817
[22] Peterkop R 1971 *J. Phys.* B **4** 513
[23] Rau A R P 1971 *Phys. Rev.* A **4** 207
[24] Al-Hagan O, Madison D H, Murray A J, Kaiser C and Colgan J 2010 *Phys. Rev. A* (submitted)
[25] Al-Hagan O, Kaiser C, Murray A J and Madison D H 2009 *Nature Phys.* **5** 59
[26] Bray I and Colgan J *Private communication* (2009)
[27] Clementi E, Raimondi D L and Reinhardt W P 1967 *J. Chem. Phys.* **47** 1300
[28] Williart A and Garcia G 2001 *Phys. Scripta* **64** 343

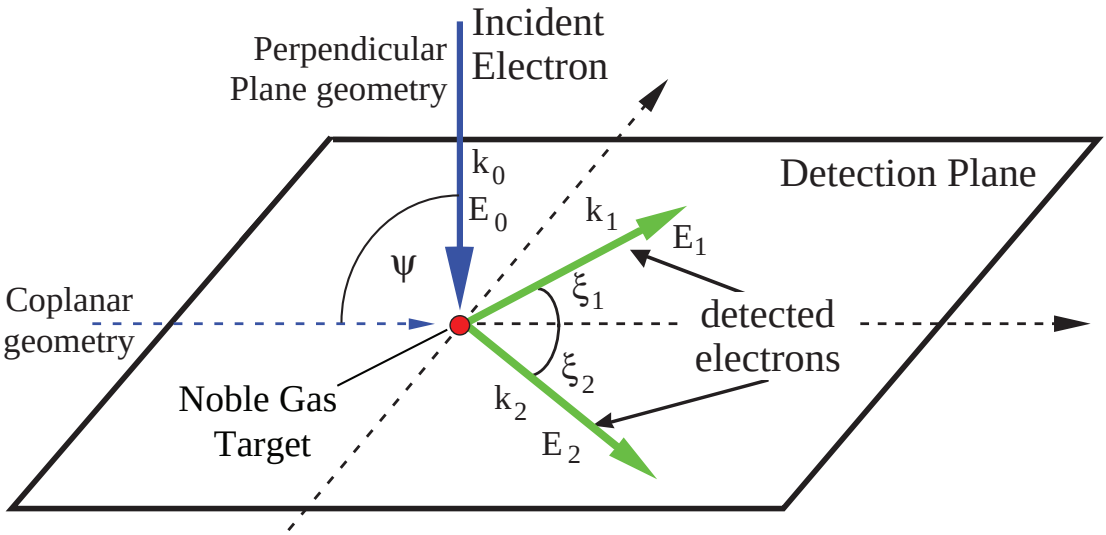

FIG 1. The experimental geometry adopted in Manchester. The incident electron can move from the coplanar geometry ($\psi = 0°$) to the perpendicular plane ($\psi = 90°$), the outgoing electrons are measured in the detection plane. For the data presented here, the perpendicular plane was chosen, so only the mutual angle $\phi = \xi_1 + \xi_2$ is relevant.

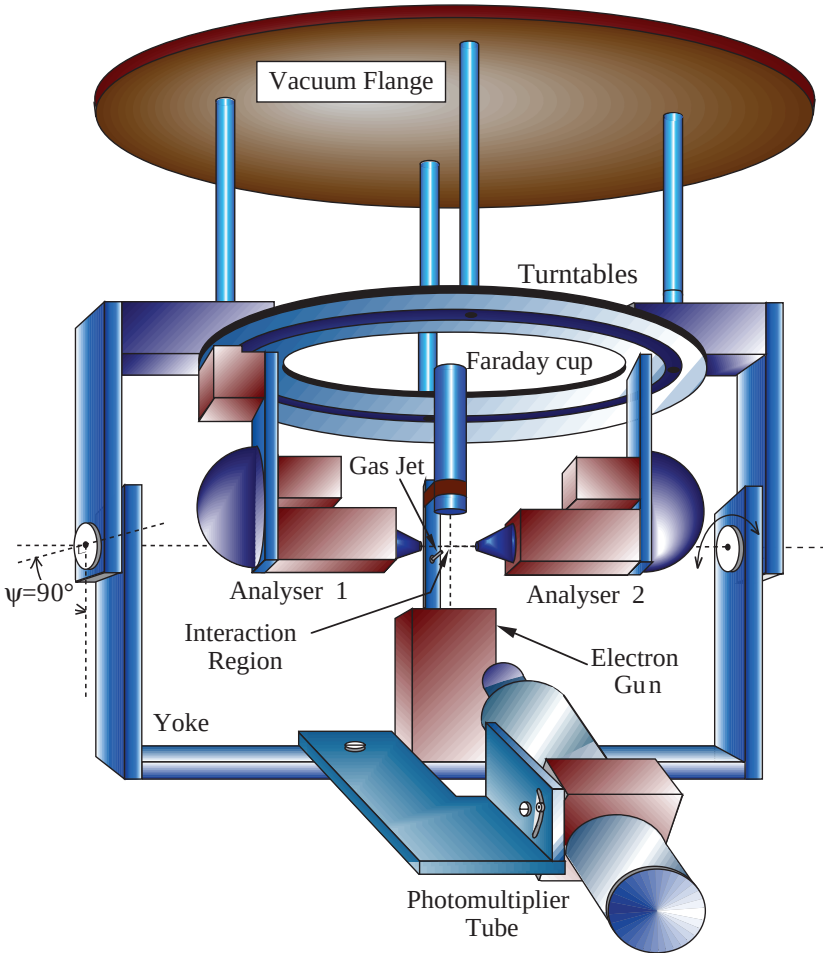

FIG 2. The (e,2e) spectrometer used in these experiments, configured in the perpendicular plane. For details, see text.

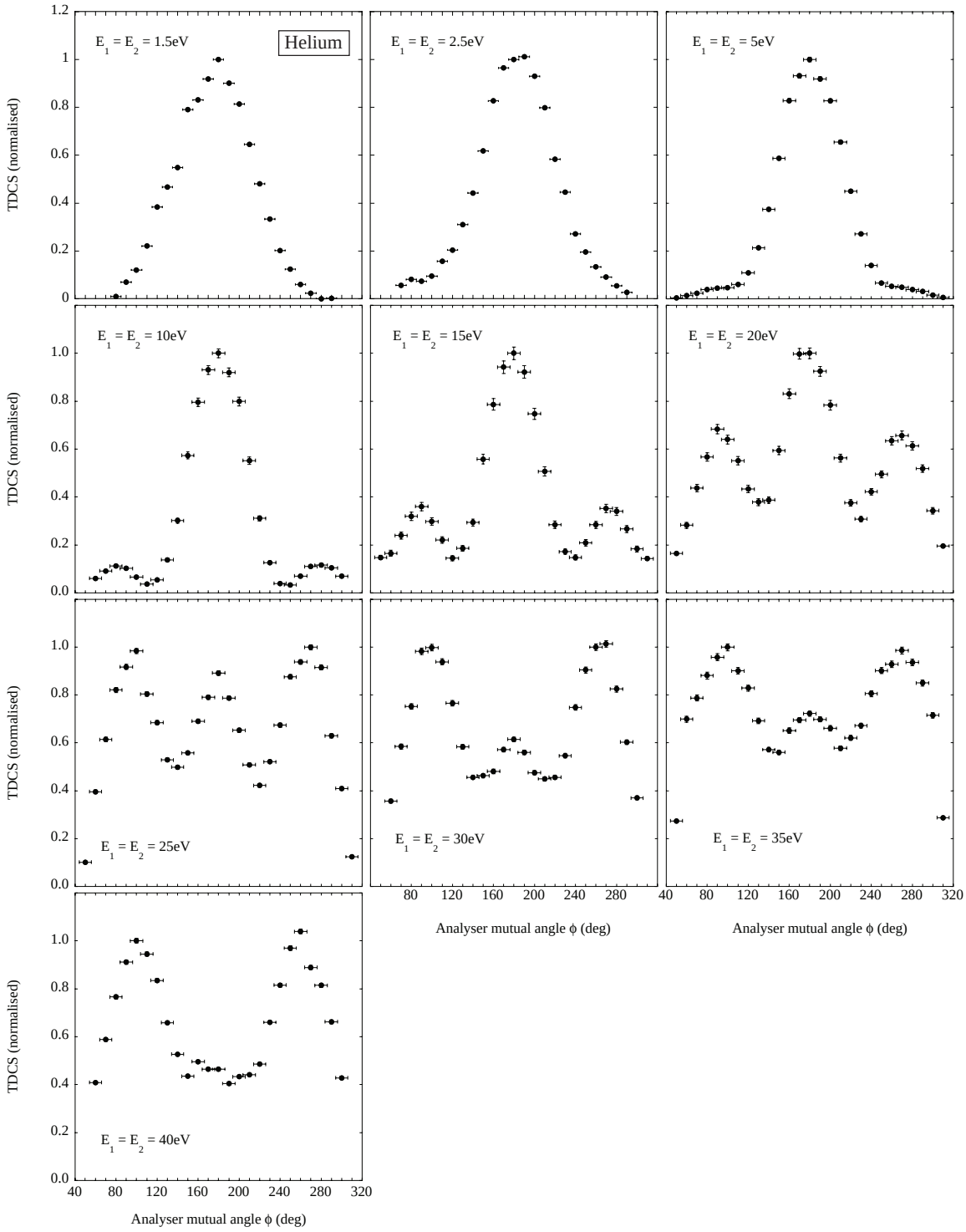

FIG 3. Experimental results for the ionization of helium in the perpendicular plane, with incident energies ranging from 3eV to 80eV above the ionization potential for this target. For details, see text.

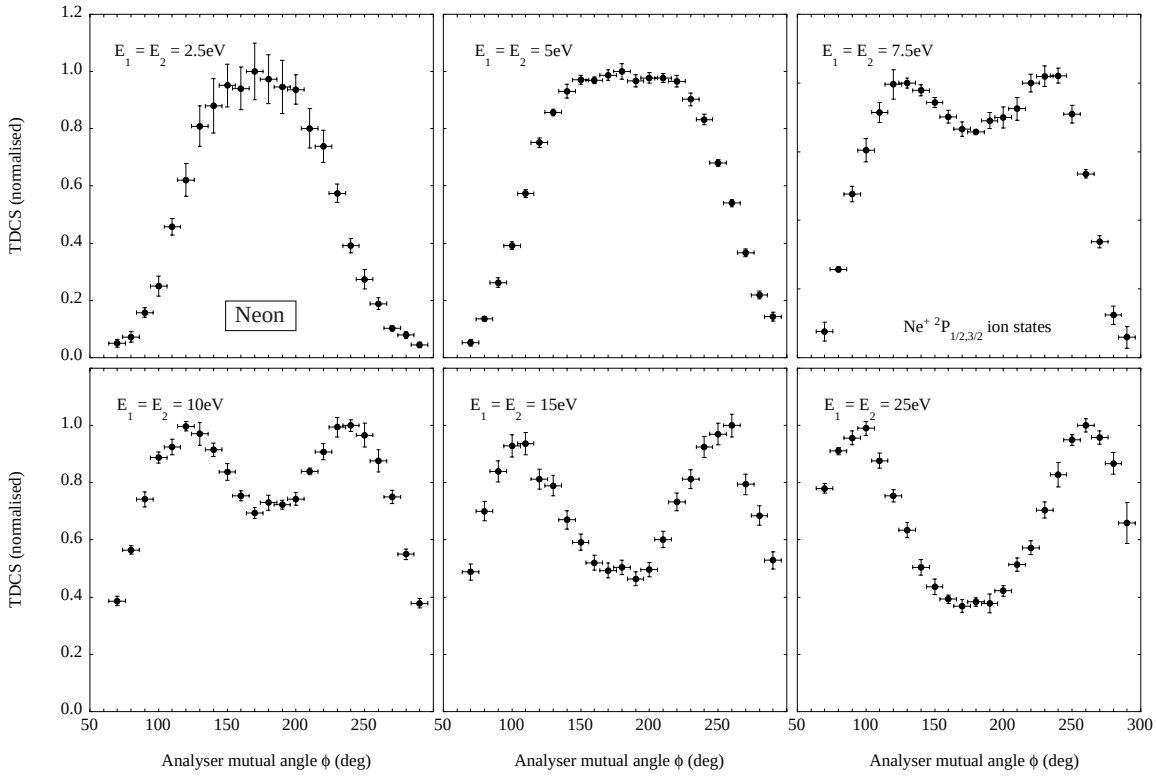

FIG 4. Experimental results for the ionization of neon in the perpendicular plane, with incident energies ranging from 5eV to 50eV above the ionization potential for this target. For details, see text.

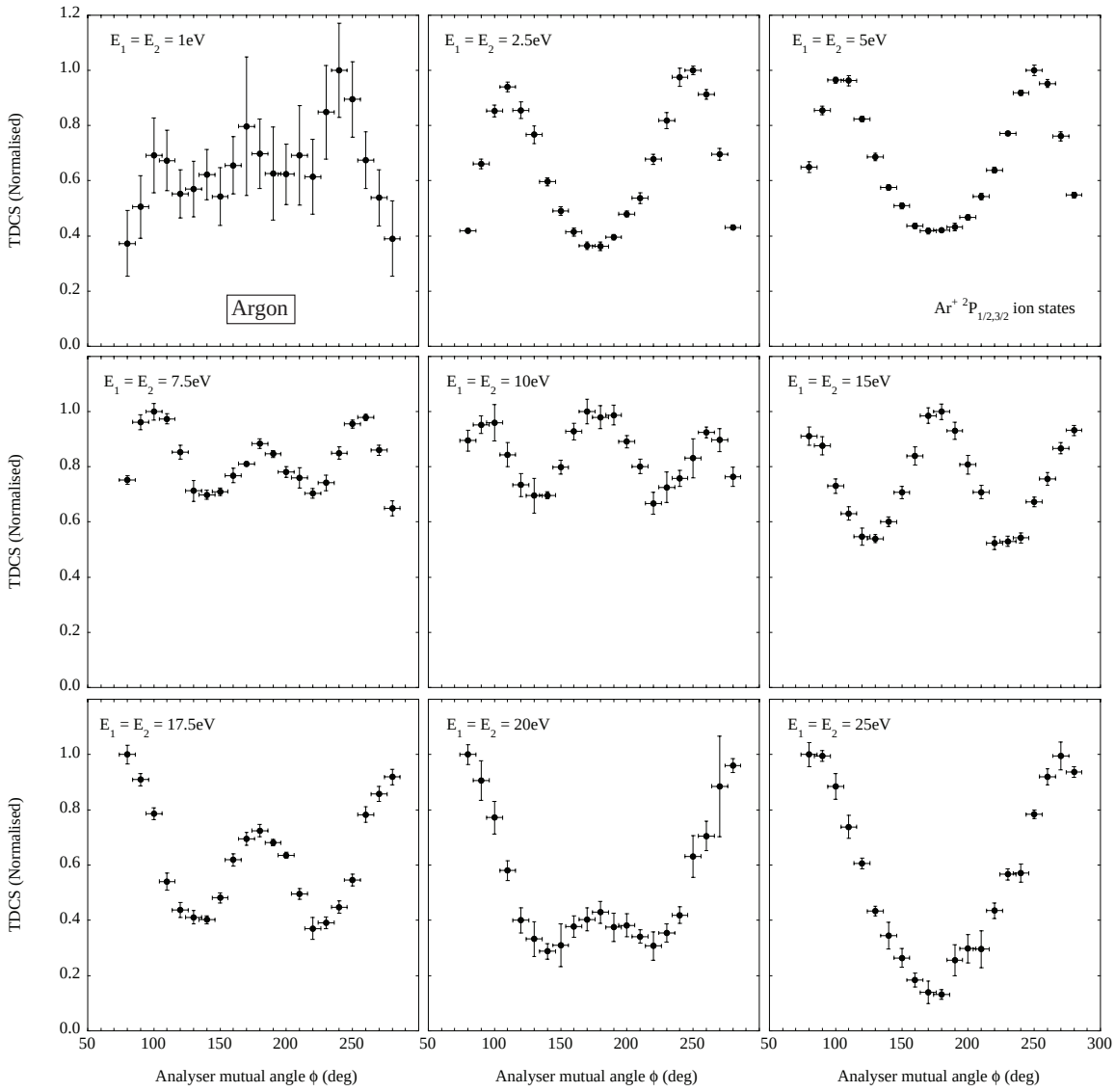

FIG 5. Experimental results for the ionization of argon in the perpendicular plane, with incident energies ranging from 2eV to 50eV above the ionization potential for this target.

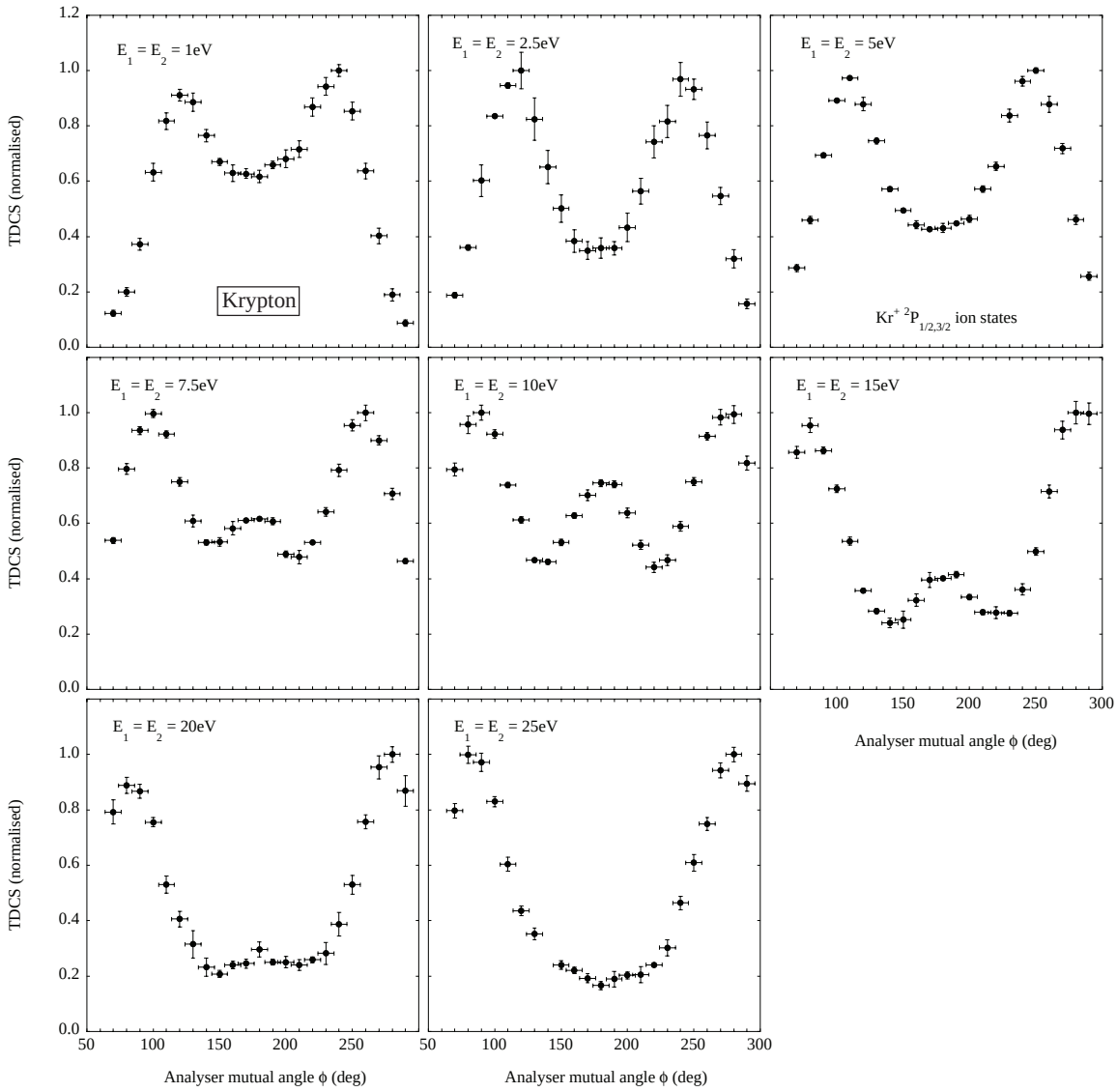

FIG 6. Experimental results for the ionization of krypton in the perpendicular plane, with incident energies ranging from 2eV to 50eV above the ionization potential for this target.

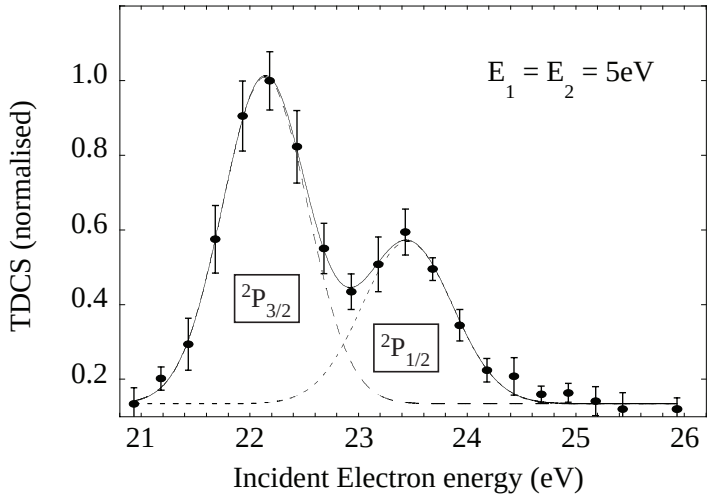

FIG 7. Energy loss spectrum for the ionization of xenon in the perpendicular plane, with incident energy 10eV above the ionization potential, showing the resolution of the $^2P_{3/2}$,$^2P_{1/2}$ ionic ground states. The data are fitted to two Gaussians, showing that contamination from each ionic state is <10% when the spectrometer is set to each peak in the cross section.

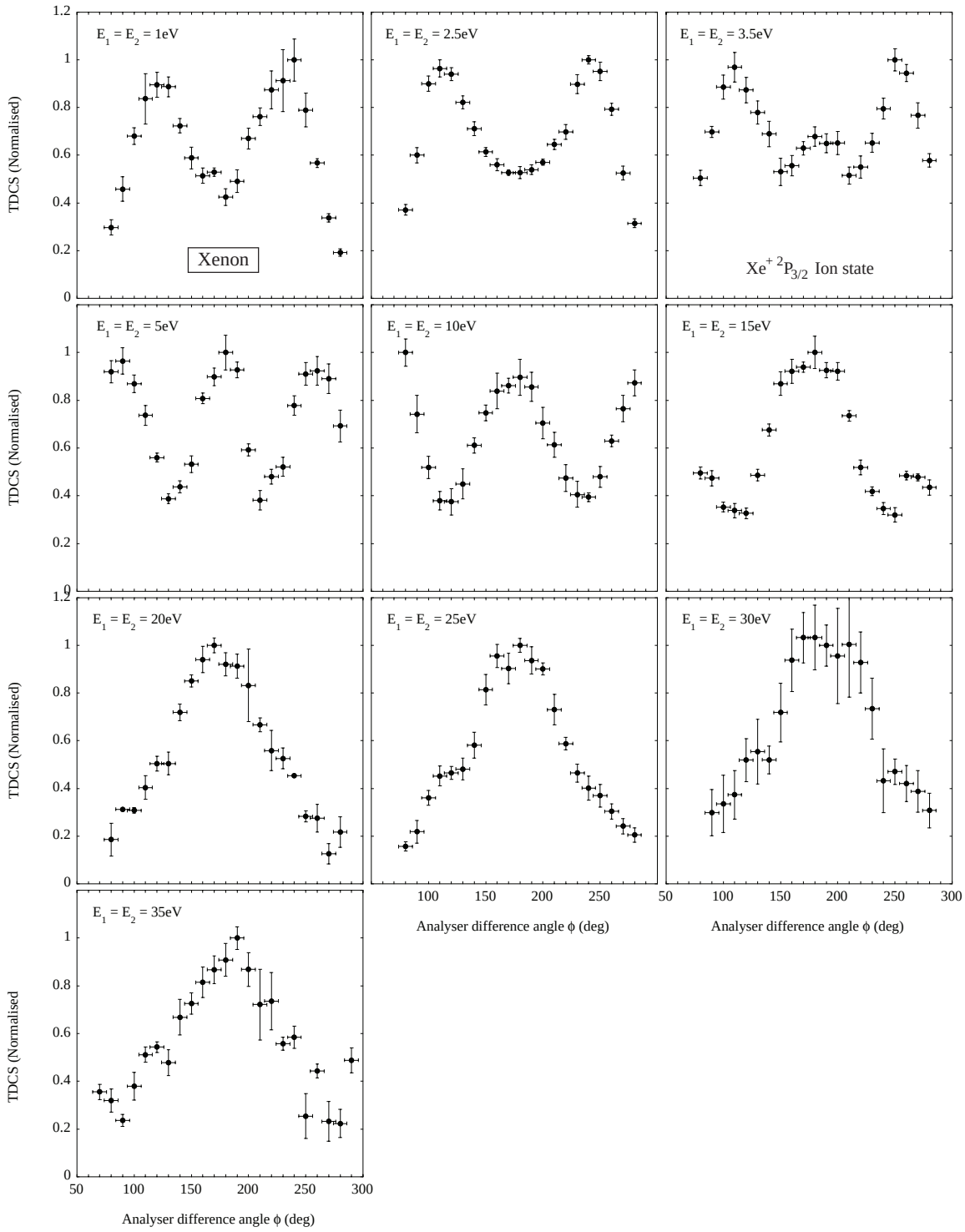

FIG 8. Experimental results for the ionization of xenon taken in the perpendicular plane, with incident energies ranging from 2eV to 70eV above the ionization potential for this target. For Energies up to 30eV above the IP the results represent those of the resolved $^2P_{3/2}$ ionic ground state. At higher energies the data measured has contributions from both ion states, but is expected to be dominated by the $^2P_{3/2}$ state.

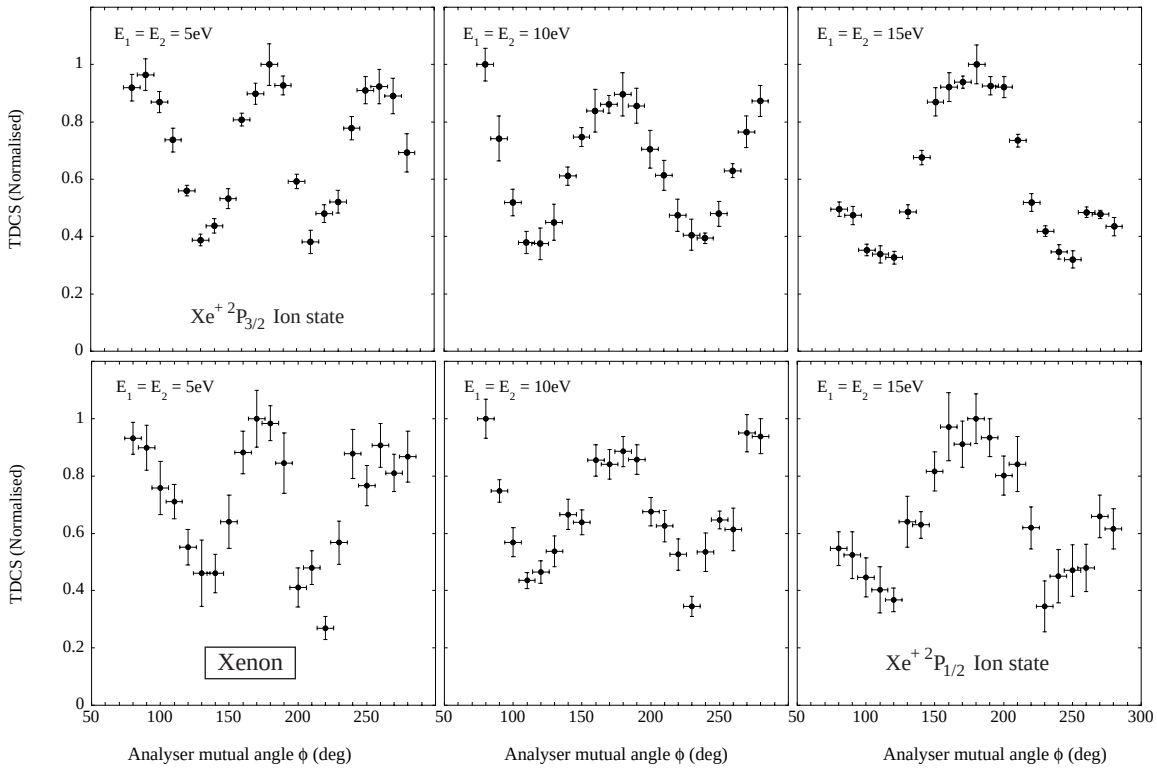

FIG 9. Experimental results for the ionization of xenon resulting in the $^2P_{1/2}$ (top panels) and $^2P_{3/2}$ (bottom panels) ionic ground states taken in the perpendicular plane, with incident energies ranging from 10eV to 30eV above the ionization potential for this target. The shapes of the DCS to the $^2P_{1/2}$ ionic ground state are very similar to those obtained for ionization to the $^2P_{3/2}$ ionic ground state at the same energies given in figure 8, as reproduced here.

Table 1. Calculated atomic radii and static polarization of the targets under study.

Target	**Atomic Radius (pm)** [27]	**Static Polarization (** a_0^3 **)** [28]
helium	31	1.38
neon	38	2.68
argon	71	11.1
krypton	88	17.7
xenon	108	27.0